Easy-to-Assemble and Adjustable Coaxial Flow-Focusing Microfluidic Device for Generating Controllable Water/Oil/Water Double Emulsions: Toward Templating Giant Liposomes with Different Properties

Kristian Torbensen and Ali Abou-Hassan*

Sorbonne Universités, UPMC Université Paris 06, Laboratoire Physico-chimie des Electrolytes et Nanosystèmes Interfaciaux (PHENIX), UMR 8234, équipe Colloïdes Inorganiques, Bat F(74), case 51, 4 place Jussieu, F-75252 Paris Cedex 05, France

Received: 13 May 2015; accepted: 14 July 2015

Herein, an optimized microfluidic device for manufacturing encapsulating water-in-oil-in-water (w/o/w) double emulsions is reported. The adjustability of the microfluidic device allows on-demand formation of oil shells with different thicknesses during the w/o/w double emulsion formation while maintaining the same core size. This was achieved by manipulation of the separation distance between the cylindrical tubes constituting the flow-focusing part of the device, the middle flow rate of the middle phase, and the outer flow rate of the continuous phase, all at the same time. By incorporating lipids in the oil shell, the w/o/w double emulsions serve as templates for the formation of monodisperse encapsulating liposomes. Thus, liposomes with different shell properties can be generated after evaporation of the oil that can be collected either separately or pooled together in a single sample batch using only one experimental step. The w/o/w double emulsions are highly monodisperse, generated with a throughput of more than 10 Hz, having water core diameters ranging from 130 to 290 μm and different oil shell thicknesses varying from 5 to 13 μm. Moreover, double emulsions with diameters down to 10 μm are reported; however, at this size, the dispersity is less controllable. The microfluidic device is composed of commercially available parts with only minor modifications required, thus, facilitating the manufacturing of encapsulating w/o/w double emulsions.

Keywords: water/oil/water, double emulsions

1. Introduction

The study of complex biological systems such as living cells has been subject to research for more than a century, resulting in a profound understanding of transport phenomena across cell membranes and cell metabolism, etc. The complexity of biological systems, often having a nonlinear response to external and internal manipulation, and the handling of living cells had led to the search for more simple and manageable model systems. In this context, giant unilamellar vesicles (GUVs) composed of self-assembled amphiphiles have proven invaluable in mimicking cellular structures [1]. In particular, the use of phospholipids as amphiphiles in the construction of artificial cellular membranes, i.e., liposomes [2, 3], constitutes an important class of structures as these membranes are easily doped, e.g., with proteins [4, 5], providing model systems for biological pathways of signal transduction and membrane transport [6]. Moreover, GUVs not only serve as synthetic model systems mimicking biological cells [7] but also play a major role in recent developments of carriers of active material in drug delivery systems [8–10] and as encapsulating agents in the food industry [11]. These versatile applications of GUVs have motivated researchers to develop different methodologies to control their elaboration.

Traditionally, GUVs are generated by hydration of dried lipid films – with (electroformation) or without a voltage potential [12–14] – or in bulk solutions followed by membrane extrusion [15, 16]. However, the as formed vesicles often lack monodispersity and/or the product yield is relative low. More recently, new techniques such as pulsed jet flow [17, 18] and, with the development of soft lithographic methods [19], microfluidic devices have been applied in the formation of lipid vesicles. In particular, microfluidics, i.e., the manipulation of fluids on the micrometric scale, has proven an excellent technique for generating double emulsion for GUV encapsulation. The drawbacks of previous techniques are here overcome by using flow-focusing microfluidic devices with high channel resolution achieved either by a lithographic approach [4, 20] or by coaxial assemblies of capillary tubes [5, 10, 21–23]. However, limitations to present designs still exist since the geometry of these devices is fixed once the cast or assembly is completed. Although some variations in the vesicle size and lamellarity can be obtained by changing the volumetric flow rates and the radius of the capillary dimensions [5, 21], these devices have no inherent option for changing the geometry of the flow-focusing part which is a crucial parameter for optimization of the vesicle design. It is important to note here that the initial products formed by the aforementioned microfluidic devices are in fact water-in-oil-in-water (w/o/w) double emulsion drops that only constitute a template for the actual vesicles. Only upon dewetting or evaporation of the volatile oil phase is the liposome membrane formed [22, 24]. In this context, controlling the thickness of the oil film in the double emulsion drops is crucial for governing the final lamellarity of the vesicle, i.e., formation of uni- or multilamellar shells or shells comprised of aggregated material [5, 24–26].

Herein, we present an optimized microfluidic device combining all together the different technical advantages reported separately for droplet [27], double emulsion [21, 28], and vesicle [5, 29] formation. We added, in a combing design, the ability of adjusting the device geometry during (i.e., under continuous flow) w/o/w double emulsion formation. This adds a new degree of freedom to accompany volumetric flow rate variations in order to increase control over the vesicle formation and characteristics, e.g., size, monodispersity, and lamellarity. On one hand, we demonstrate the ability of generating monodisperse encapsulating liposomes from w/o/w double emulsion templates, having the same water core size but different oil shell thicknesses. We assume that, after evaporation of the oil shells of different thicknesses, and at the same phospholipid concentration, increasing (respectively decreasing) the thickness of the oil layer will result in liposomes of different membrane properties (lamellarity, permeability, etc.). Such a control on the membrane properties can be ideal for a broad variety of studies, e.g., on the effect of membrane on chemical communication [30] and membrane sequestering and membrane permeation of bioactive molecules for modelling drug delivery systems [31]. In a biomimetic approach, e.g., modelling living cells, indeed, a unilamellar structure is preferred. However, for compartmentalizing purposes,

* Author for correspondence: ali.abou_hassan@upmc.fr

DOI: 10.1556/1846.2015.00023

First published online: 04 October 2015

it might be desirable to increase the vesicle stability by generating multilayered membranes. Although the sizes of the generated vesicles are too large for real drug delivery applications, for the aforementioned purposes, the size of the generated vesicles might come in handy as individual vesicles can be monitored optically and spectroscopically. On the other hand, the adjustability enables on-demand change of the liposome lamellarity, resulting in monodisperse vesicles with different shell properties within the same batch. This provides a versatile and reliable platform for screening trials for investigation of membrane transport phenomena, release conditions of delivery systems, etc. Furthermore, our device enables mixing of liquid phases prior to the vesicle encapsulation process, thus preventing premature aging of chemical reactions intended to occur solely within the vesicles.

2. Results and Discussion

Our device is constituted of coaxially aligned glass tubes of various dimensions and geometry. First, a single or two fused (using epoxy resin) polyimide coated 150/50 μm (outer diameter [OD]/inner diameter [ID]) glass capillary tubes (Polymicro) are inserted into a cylindrical 1/0.5 mm (OD/ID) borosilicate tube (Drummond Scientific). The borosilicate tube was narrowed in one end for enhanced flow focusing (see below) by exposing the tube orifice to a butane flame while rotating the tube. The inner wall and the orifice of this tube were rendered hydrophobic using 2% (v/v) trichloro(1*H*,1*H*,2*H*,2*H*-perfluorooctyl)silane (Sigma-Aldrich) in toluene, rinsed with toluene and dried overnight at 70 °C to obtain desired wetting properties. These tubes are in turn inserted into a square borosilicate tube 1.25 × 1 mm (outer/inner side length, Vitrocom), the principal illustrated in Figure 1A. Depending on the solution (s) to encapsulate, one or more tubes can be used. However, the use of two tubes (or more) is mandatory when there is a need to separate chemicals, preventing them from premixing and reacting before encapsulation inside the double emulsions. A second cylindrical borosilicate tube, likewise flame treated and serving as the vesicle collector tube, was inserted from the opposite end of the square tube, and the two cylindrical tubes were positioned with the narrowed orifices in close position followed by positioning of the two inner most fused capillary tubes close to the orifice of the left cylindrical tube (see Figure 1B). All glass tubes were assembled using T-crosses (P-727, Upchurch Scientific), ferrules (F-331, Upchurch Scientific), and pieces of 1/3 mm (OD/ID) silicon tubing (Tygon Versilic Silicon Tubing, Sigma-Aldrich) and mounted on a Plexiglas stand as displayed in Figure 1C. All parts required for the device are shown in Figure S1 (see Supporting Information). The setup allows injection of fluids into the innermost capillary tubes, the left most cylindrical tube and from both ends of the square tube as illustrated in Figure 2. Additionally, the separation distance between the cylindrical tubes, *d*, and thus the geometry of the flow-focusing part, can be varied by turning the left most ferrule fitting as illustrated by the red arrow in Figure 1C. The soft silicon tube sealing allows for changing reversibly, and without any leakage, the distance by several hundreds of micrometers, which can be done in a controlled manner when monitored by optical microscopy. The close joining of the two innermost capillary tubes results in instantaneous merging of the aqueous

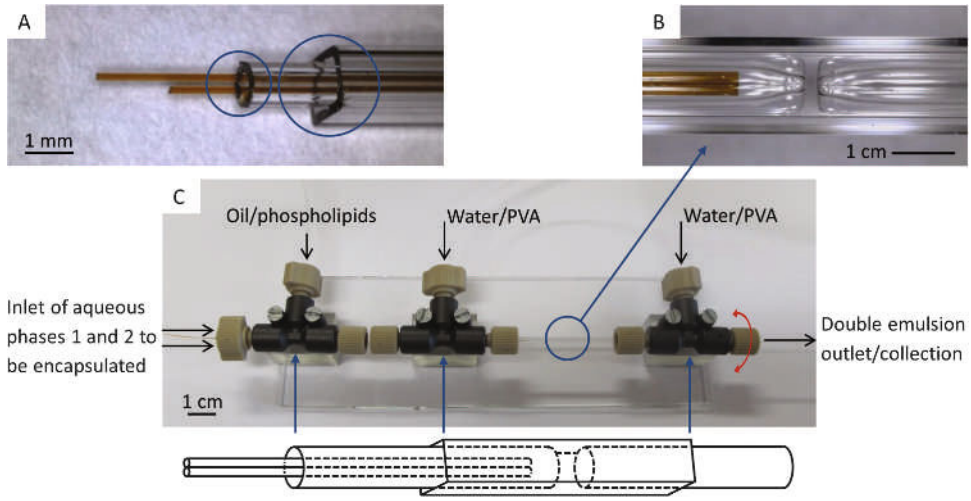

Figure 1. (A) Image demonstrating the concept of coaxial alignment of tubes with various diameters and geometries. The circles highlight the flow entries enclosed in the T-crosses enabling the coaxial flow of the oil phase along the two innermost capillaries and the aqueous solution of polyvinyl alcohol (PVA, 2% wt, Mw 18 kDa) solution in the corners of the square tube, the latter from both ends. (B) Close-up of the flow-focusing part of the microfluidic device showing the two innermost fused capillary tubes and the narrowed cylindrical tubes enclosed in the outer square tube and (C) the complete assembled microfluidic device mounted on a Plexiglas stand, together with a sketch of the assembled tubes

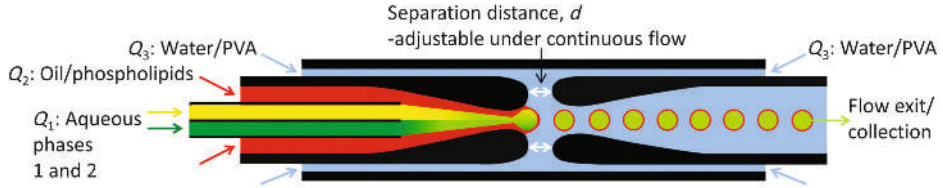

Figure 2. Schematic illustration of the microfluidic device for generating w/o/w double emulsions. A simple emulsion (w/o middle phase, light green) of two mixed aqueous phases (yellow and green, total volumetric flow Q_1) is being formed in the oil containing phospholipids (red, volumetric flow rate Q_2) in the left inner capillary tube just prior to the encapsulation. Breakup and reemulsification of the w/o middle phase is effectuated upon encountering the outer aqueous phase, flowing in from the corners of the square tube with total volumetric flow rate of Q_3, forming monodisperse w/o/w double emulsion drops (light green in red circles) in the right capillary tube. The white arrows indicate the geometric adjustability of the device

phases upon forming a coherent aqueous flow engulfed by the oil phase. In principal, this protocol enables insertion of several fused inner tubes allowing mixing of multiple phases prior to emulsification.

As stated previously, flow-focusing devices reported so far have been described to control the size of the final vesicles by controlling the size of the w/o/w double emulsions. This was achieved by varying the ratio of the volumetric flow rate of the outer flow (Q_3) to the oil middle flow rate (Q_2), which not only varied the thickness of the oil layer but also affected the size of the inner aqueous core. Similar results were obtained in our device for a fixed geometry; the size of the double emulsions (core and oil shell) decreased when Q_3/Q_2 increased.

However, our main objective is to prepare double emulsions with same core sizes but with variable oil shell thicknesses, which may result, after evaporation, in different membrane lamellarity. Our work is mainly motivated by our recent work on chemical communication between vesicles encapsulating chemical information [30].

To demonstrate the versatility of the microfluidic device in varying the thickness of the oil shell, and thus the lamellarity of the final liposomes, while maintaining the size dispersity (same core size) of the liposomes, we generated w/o/w double emulsions with different geometric configurations of the device, i.e., different distances, d, separating the orifices of the cylindrical tubes, as displayed for two cases by the optical micrographs in Figure 3 (multimedia view). The left row, Figure 3A–C, and the right row, Figure 3D–F, show the device with d = 122 μm and 276 μm, respectively. The inner aqueous phase was injected with a volumetric flow rate of Q_1 = 15 μL/min and was formed in situ by mixing two aqueous solutions containing 2% (w/w) polyvinyl alcohol (PVA), with a dynamic viscosity (η) at 20 °C of 1.63 mPas (measured with an automated micro viscometer, Anton Paar), of which one contained 10 mM ferroin as a dye marker. The middle oil phase was injected with different volumetric flow rates of Q_2 and was composed of a solution of the phospholipid 1,2-dimyristoyl-*sn*-glycero-3-phosphocholine (DMPC; 1% [w/w]) dissolved in a mixture of the volatile solvents cyclohexane–chloroform (volume ratio 2:1). The experiments were performed at 20 °C, thus, maintaining the DMPC in the gel state [30]. The outer phase was an aqueous solution containing 2% (w/w) PVA and was injected at different volumetric flow rates of Q_3. All volumetric flows were controlled using syringe pumps (KD Scientific). The PVA serves both to increase the viscosity for enhanced flow focusing and to increase the stability of the double emulsions [5]. When the viscosity ratio of the outer phase to the inner phase was below 1, only laminar flow can be observed and no jetting or dripping occurred. However, when the viscosity ratio was ≥1, double emulsion is observed due to Rayleigh–Plateau instabilities. The instantaneous merging of the co-flow of the two innermost capillaries is driven by a decrease in surface tension upon encountering the hydrophobic oil phase, thus, forming a simple water-in-oil emulsion, as displayed in Figure 3A and 3D. The drop-shaped inner aqueous phase is clearly seen engulfed by the coaxially flowing oil phase, the latter forming a meniscus at the hydrophobic orifice of the left capillary tube, just prior to formation of the w/o/w double emulsion in the right capillary tube. The addition of a dye in one of the innermost capillary tubes clearly demonstrates the instant merging of the two aqueous phases. Figure 3B and 3E displays the w/o emulsion just after breakup of the inner aqueous phase, now entirely engulfed by the oil meniscus, and just prior to entering the left collection tube. The natural hydrophilic character of the borosilicate glass ensures wetting of the left capillary tube by the outer aqueous phase, thus facilitating the w/o/w emulsification. Figure 3C and 3F shows the final breakup of the oil phase forming the w/o/w double emulsion. The increased orifice separation, with concomitant increased flow rate of the outer aqueous phase, causes the oil phase to break up in the dripping regime more rapidly and closer to the orifice of the left tube, thus generating a much thinner oil film separating the encapsulated and the outer aqueous phases. An increase of the outer aqueous flow rate, without changing the separation distance *(d),* not only resulted in a larger separation of the double emulsions in the collection tube but also decreased the size of the w/o/w double emulsions, thus disrupting the overall size dispersity. When the flow rate of the outer aqueous phase was kept constant and the separation distance was increased, the size of the double emulsions decreased and a transition to laminar regime can be observed for $d \geq 350$ μm, thus leading to nonformation of double emulsions. Thus, it is clear that, to prepare double emulsions of same inner core size and different oil thicknesses, the orifice separation and the flow rates of the middle oil phase and the outer aqueous phase have to be changed simultaneously. The throughput, i.e., the generation

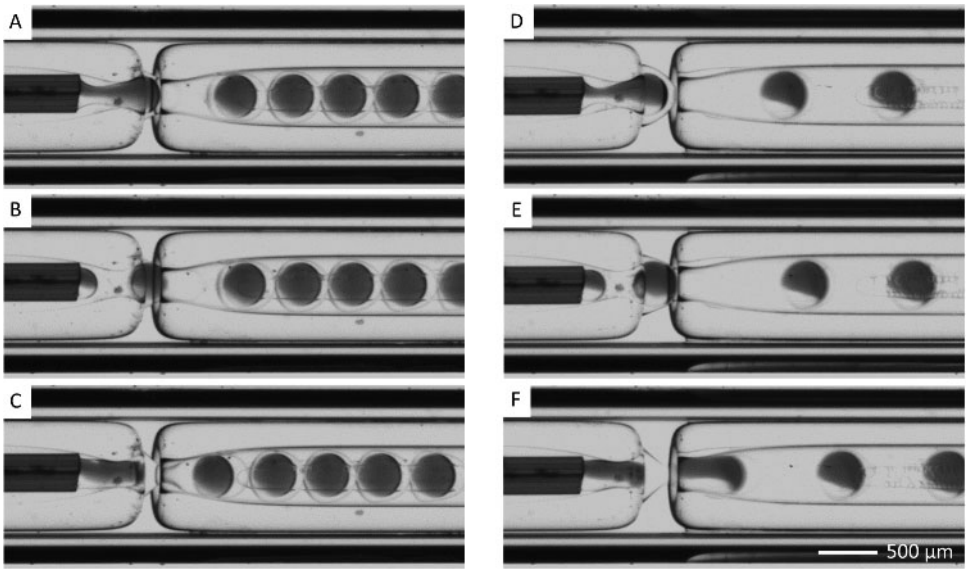

Figure 3. Snapshots showing w/o/w double emulsions generation in the flow-focusing part of the adjustable microfluidic device obtained at same Q_1 = 30 μL/min for the inner phase while changing at the same time the orifice separation *(d),* Q_2 of the oil phase, and Q_3 of the outer aqueous phase. (A–C): d =122 μm, Q_2 = 10 μL/min, and Q_3 = 10 μL/min, resulting in a thick oil shell in the generated w/o/w double emulsions. (D–F): d = 276 μm, Q_2 = 3 μL/min, and Q_3 = 50 μL/min resulting in a barely visible oil shell separating the encapsulated and the outer aqueous phases (multimedia view)

frequency, of the w/o/w double emulsions is 14 and 16 Hz for the setup shown in Figure 3A–C and Figure 3D and E, respectively.

The effect of changing the geometry of the flow focusing part of the device on the resulting oil shell thickness was investigated by optical and fluorescence microscopy using the organic soluble fluorophore rhodamine B (Sigma-Aldrich). The w/o/w double emulsions were generated in a microfluidic device mounted with a single inner most capillary tube. The volumetric flow rates of the different flows were Q_1 = 30 μL/min for the inner aqueous phase composed only of an aqueous PVA solution (2% [w/w]), Q_2 = 3–10 μL/min for the middle phase composed of DMPC (1% [w/w]) in a mixture of cyclohexane–chloroform solvents (2:1 [*v*:*v*] and containing 0.5% [w/w with respect to DMPC] rhodamine B) and Q_3 = 10–50 μL/min for the outer aqueous PVA solution (2% [w/w]). The separation distance, *d*, between the orifices of the cylindrical tubes was varied between 100 and 300 μm. Different types of w/o/w double emulsions were collected on a glass slide mounted with a 65-μL frame reservoir and left for 10 min. This resulted in the double emulsions to settle in one layer on the glass slide due to the density of the oil phase being slightly higher than the outer aqueous matrix. The degree of oil phase evaporation is expected to be rather low at the experimental temperature of 20 °C at this time scale; thus, the membranes are believed to contain a considerable amount of the organic solvents.

Figure 4A–D displays optical and fluorescent micrographs of four examples of such batches of double emulsions, generated with orifice separations, *d*, of 276, 201, 162, and 122 μm, middle fluid volumetric flow rates, Q_2, of 3, 5, 7, and 10 μL/min and outer fluid volumetric flow rates, Q_3, of 50, 30, 20, and 10 μL/min, respectively. As can be seen from Figure 4A–D, the spatial density of the double emulsions increases with decreasing values of Q_3, and due to their high monodispersity, double emulsions tend to organize into hexagonal packed clusters. The average diameters of the double emulsion measured on at least 100 double emulsions for the different conditions are 286.4 ± 2.4, 285.0 ± 1.6, 290.6 ± 2.1, and 287.5 ± 2.0 μm, respectively, which confirm the versatility of the system to produce double emulsions with same core sizes and with high monodispersity.

Figure 5 displays magnified optical and fluorescent micrographs along with membrane profile plots of the double emulsions displayed in Figure 4. The observed oil shell thickness, defined as the full-width-at-half-maximum of the profile plots, provides thicknesses of 5.3 ± 0.9, 8.9 ± 1.1, 10.1 ± 0.8, and 12.7 ± 1.2 μm for the double emulsions shown in Figure 5A–D, respectively (based on measurements of at least 25 double emulsions for each oil shell thickness). This gives an oil shell thickness-to-diameter ratio between 0.019 and 0.044 on going from the ultrathin shell of the double emulsion depicted in Figure 5A, to the thickest shell in Figure 5D. These values are several orders of magnitude higher than what is expected for unilamellar membrane structures and probably caused by the considerable amount of organic solvents left in the membrane. The resulting liposomes obtained after complete solvent evaporation are under current investigation.

The ability of generating double emulsions of equal core radius, *R*, with different oil shell thicknesses, *t*, is illustrated by plotting *R* and *t* as a function of the parameters changed during the generation, i.e., the middle and outer fluid volumetric flow rates, Q_2 and Q_3, and the separation distance, *d*, between the two inner capillaries. Figure 6A shows the core radius as a function of Q_3 and *d* for the four different oil shell designs described above. The small size variation shows overall high size dispersity for all four types of double emulsions. The changes in the oil shell thickness as a function of the total volumetric flow, Q_{tot}, and Q_2 are shown in Figure 6B.

Here, a linear relationship between the oil shell thickness and both the outer fluid volumetric flow rate divided by the orifice

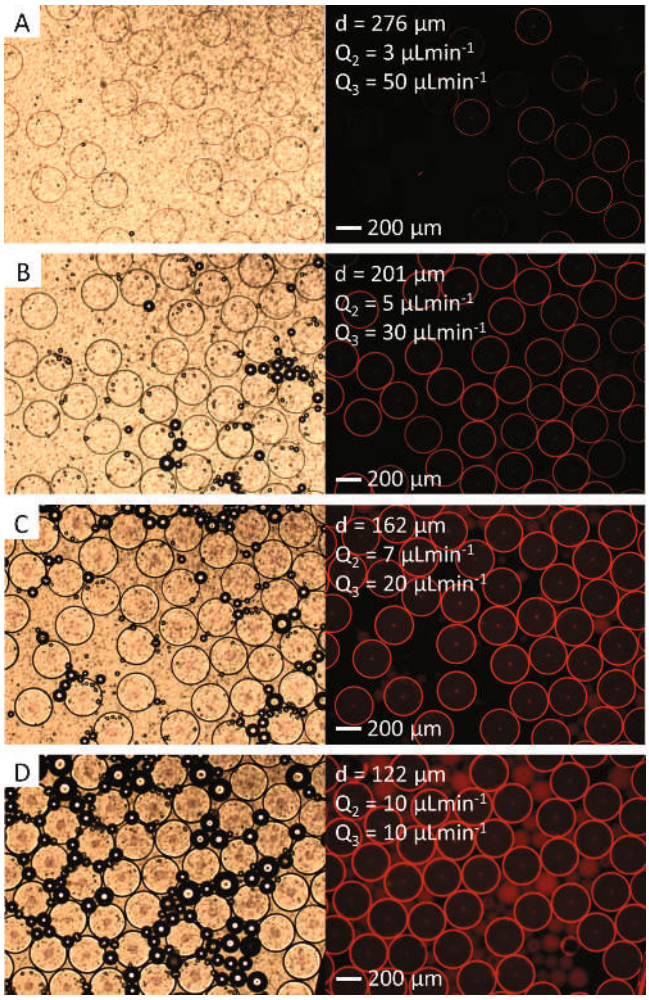

Figure 4. Optical (left) and fluorescence micrographs (right) of w/o/w double emulsions with various oil shell designs generated using constant flow rates of Q_1 = 30 μL/min for the inner aqueous solution (2% [w/w] PVA solution), varying flow rates of Q_2, the middle oil layer (DMPC–cyclohexane–chloroform phase, 1% (w/w), 2:1 [v/v]), and Q_3, the outer aqueous solution (2% [w/w] PVA solution). The DMPC was mixed with 0.5% (w/w) rhodamine B

separation distance, and the flow rate, Q_2, of the middle oil phase are observed. A theoretical model for predicting both *R* and *t* can be generated by using the frequency with which the double emulsions are formed. The mean flow velocity, *U*, in the left capillary can be calculated as the total volumetric flow, Q_{tot} (= $Q_1 + Q_2 + Q_3$), divided by the cross section, *S*: $U = Q_{tot}/S$. The frequency of formation, *f*, is then defined as the ratio *U*/*d*, where *d* is the orifice separation distance. From mass balance considerations, the core radius of the double emulsions is then defined as eq. 1:

$$R = \left(\frac{Q_1}{f}\frac{3}{4\pi}\right)^{1/3} \quad (1)$$

From eq. 1, a constant value for *R*, close to the experimentally obtained values, can be obtained by using the experimental flow rates and values for *d* close to the experimental ones, as shown in Figure 6A. Similar considerations can be used to evaluate theoretical values for the oil shell thickness, eq. 2:

$$t = \left(\frac{Q_1 + Q_2}{f}\frac{3}{4\pi}\right)^{1/3} - R \quad (2)$$

Again, as shown in Figure 6B, a good correlation is observed between the experimental values and the values predicted by the

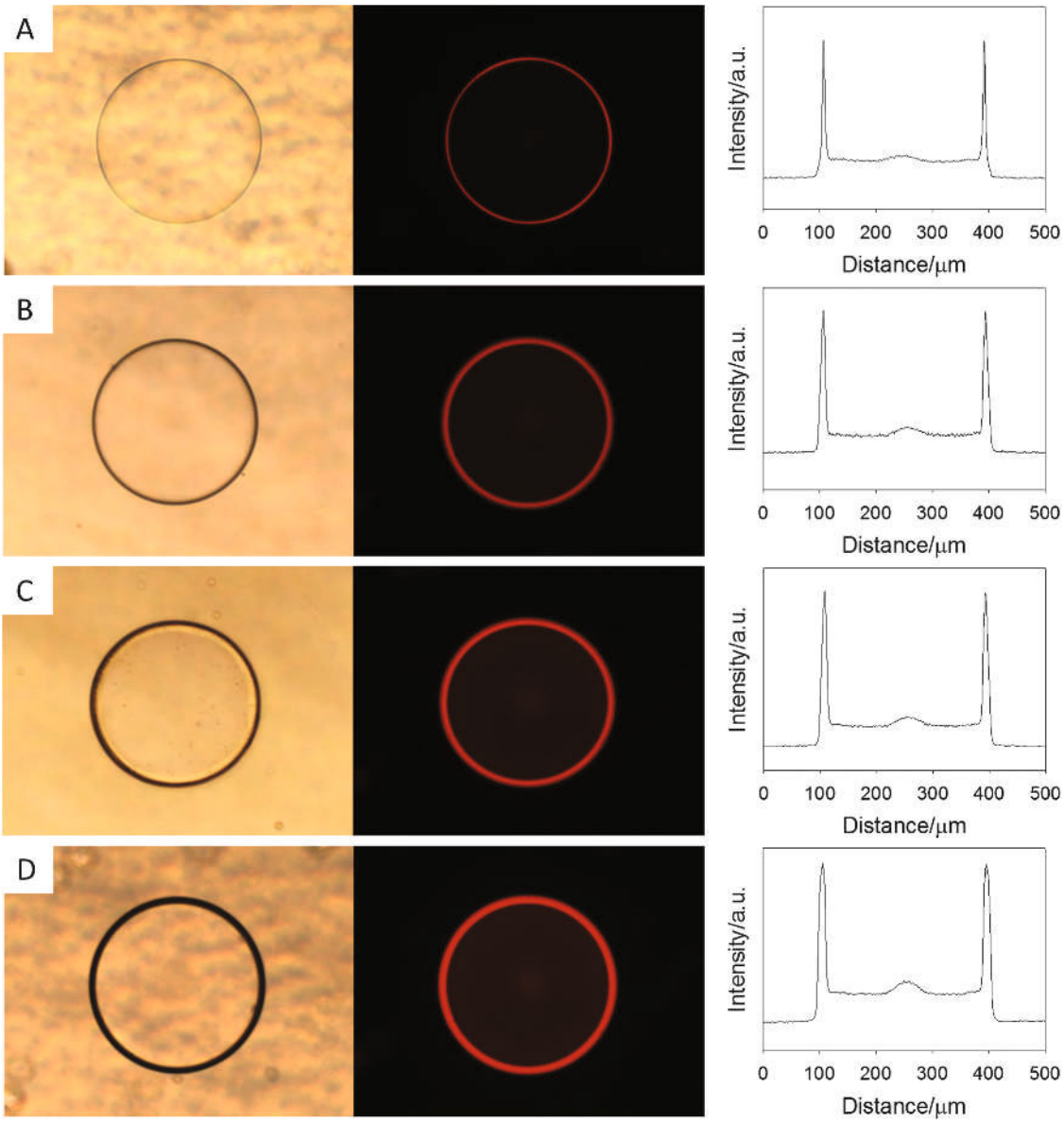

Figure 5. Optical and fluorescence micrographs and membrane profile plots (from left to right) of w/o/w double emulsions with various membrane designs collected individually. Generated using the same conditions as described in Figure 4

theoretical model. This displays the ability with which the oil shell can be designed in a controlled manner while maintaining the same core size.

As reported in literature, the size of the double emulsions and the membrane thickness can be tuned by changing the outer fluid flow rate and the ratio between the inner and middle fluid flow rates, respectively [23]. However, we experienced that simultaneously maintaining control over both the size dispersity and membrane thickness by adjusting the flow rates proved difficult. Instead, we took advantage of the possibility to easily exchange the individual parts of the device. By decreasing the inlet diameter of the inner left capillary, i.e., the inlet of the collection capillary, the double emulsion size was reduced. Examples of monodisperse double emulsions with diameters of 130 μm are shown in Figure 7. By further decreasing the inlet diameter, double emulsions with diameters down to 10 μm could be generated, however, with less control over the dispersity, as shown in Figure 8. We are currently working on optimizing the geometry of the device in order to generate monodisperse double emulsions with sizes below 10 μm.

Finally, the versatility of the device was demonstrated by the ease with which, during the w/o/w double emulsion formation, batches of monodisperse double emulsions with different oil shell thicknesses can be generated by simply sliding back and forth the left capillary tube, by turning the left most ferrule fitting in Figure 1, while adjusting the outer aqueous volumetric flow rate, as described above. The double emulsions were collected on a glass slide and left to settle for 10 min at 20 °C. Figure 9 shows optical and fluorescent micrographs of an assembly of double emulsions with monodisperse size but different oil thicknesses. The ability of elaborating such assemblies enables monitoring various properties originating from the different membrane compositions, e.g., membrane transport phenomena and release properties, within the same batch in a screening approach.

3. Conclusion

We have demonstrated a new easy to assemble/disassemble and robust design for a microfluidic device with adjustable geometry for generating monodisperse w/o/w double emulsion templates for encapsulating liposomes with a diameter range of 130 to 290 μm with a throughput of more than 10 Hz. Double emulsions down to 10 μm were generated; however, at this size, the dispersity was lower. The oil shell thickness of the double emulsions can be varied from ultrathin shells, herein reported

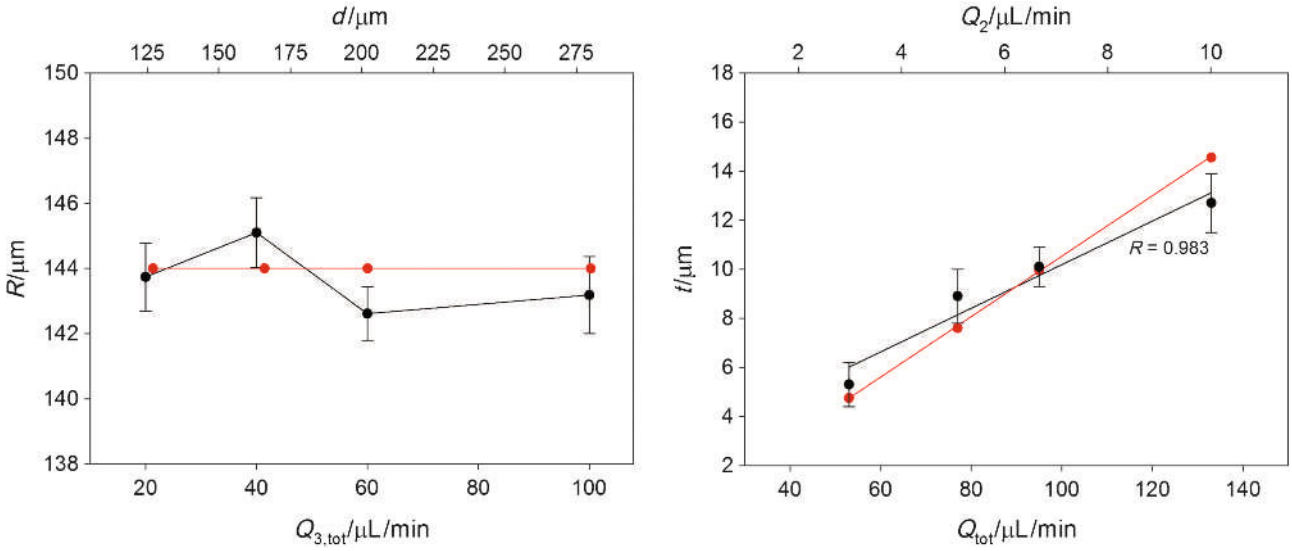

Figure 6. Plots of (A, black trace) the double emulsion size and (B, black trace) the oil shell thickness as a function of the total outer volumetric flow rate, $Q_{3,tot}$, and the orifice separation distance, d. Values deduced from the double emulsions depicted in Figures 4 and 5. Red traces in both figures show theoretical calculations based on eqs. 1 and 2

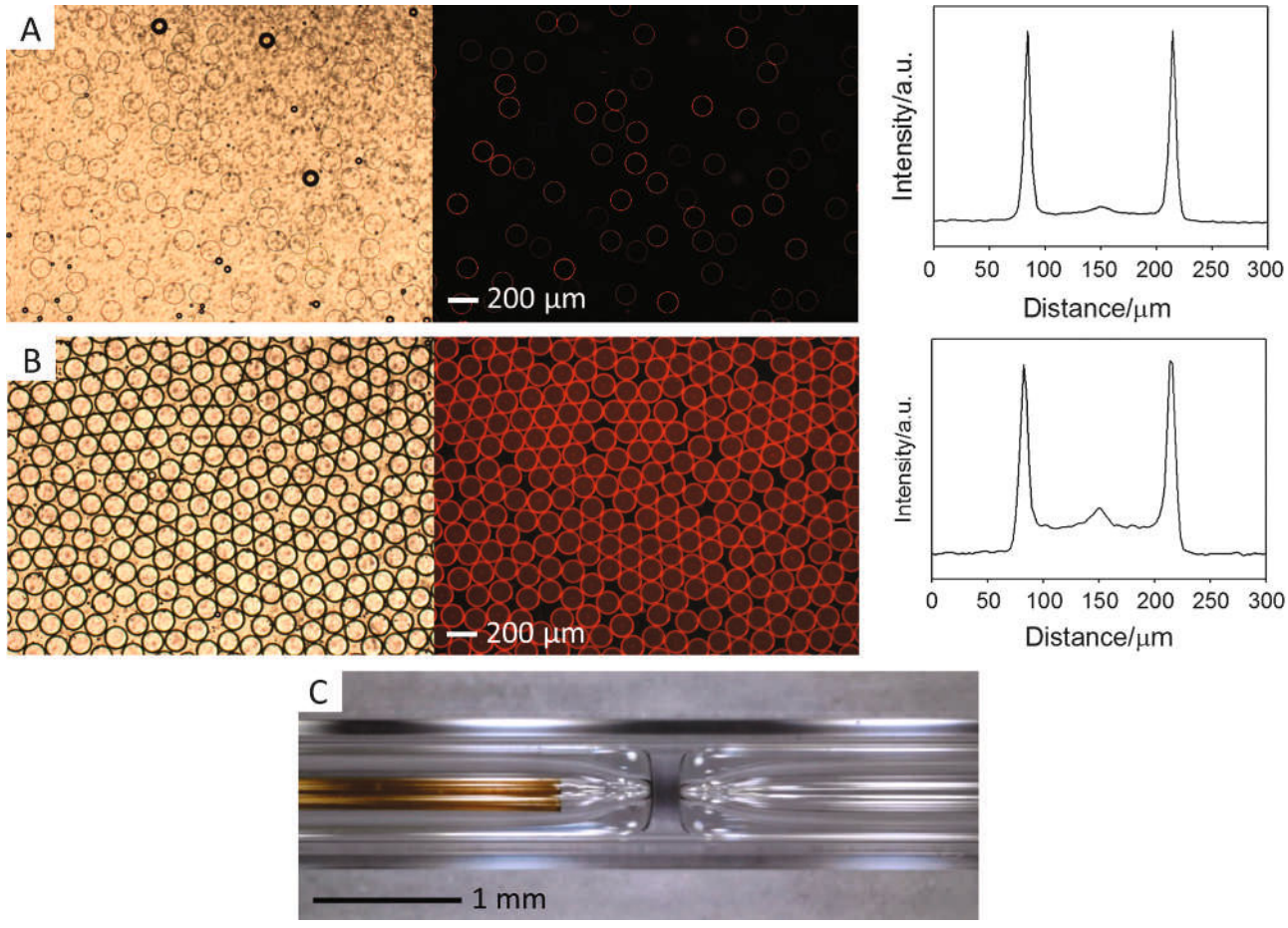

Figure 7. Optical, fluorescence micrographs, and profile plots (from left to right) of w/o/w double emulsions with various oil shell designs. The double emulsion core sizes are 130.4 ± 1.7 and 132.1 ± 2.1 μm with membrane thicknesses of 6.0 ± 0.9 and 10.1 ± 0.8 μm in (A) and (B), respectively. Generated using flow rates of 30 μL/min for the inner aqueous/2% (w/w) PVA solution and 10 μL/min for the DMPC–cyclohexane–chloroform phase (1% [w/w], volume ratio 2:1), while the flow rate of the outer aqueous/2% (w/w) PVA solution was 50 and 10 μL/min and the separation distance between the two cylindrical capillary orifices was 300 and 100 μm in (A) and (D), respectively. The DMPC was mixed with 0.5% (w/w) rhodamine B. Close-up of the flow-focusing part of the microfluidic device used here is shown in (C)

down to 5.3 μm. The ease of adjusting the geometry of the coaxial design enables the formation of encapsulating liposomes with different membrane properties and high monodispersity either to be collected separately or within the same batch. The latter provides the opportunity of monitoring various effects of the membrane composition in a single sample

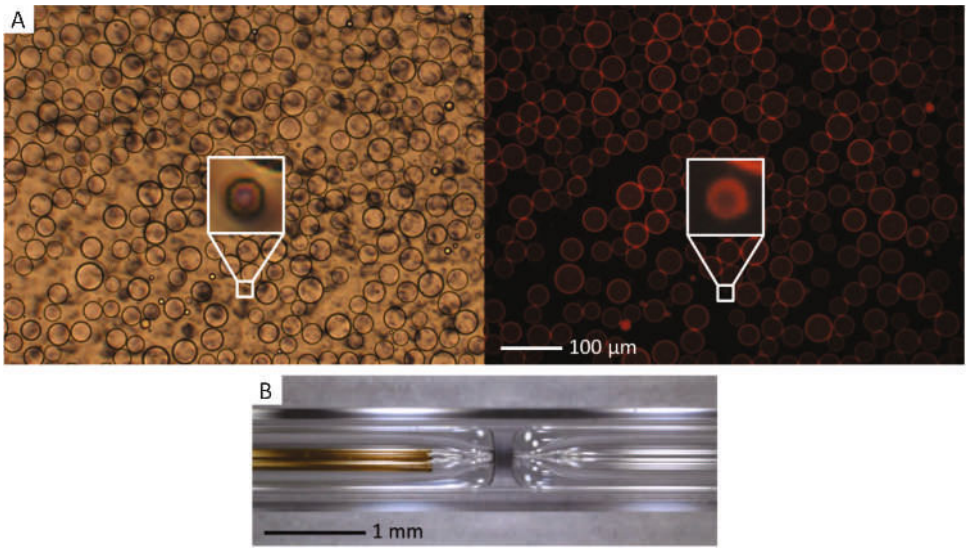

Figure 8. (A) Optical and fluorescence micrographs (from left to right) of w/o/w double emulsions with various oil shell designs. The double emulsion core sizes are generally 28 to 50 µm; however, few double emulsions of below 10 µm are observed (see insert in (A)). Generated using flow rates of 30 µL/min for the inner aqueous/2% (w/w) PVA solution and 10 µL/min for the DMPC–cyclohexane–chloroform phase (1% [w/w], volume ratio 2:1), while the flow rate of the outer aqueous/2% (w/w) PVA solution was 50 µL/min and the separation distance between the two cylindrical capillary orifices was 200 µm. The DMPC was mixed with 0.5% (w/w) rhodamine B. Close-up of the flow-focusing part of the microfluidic device used here is shown in (B)

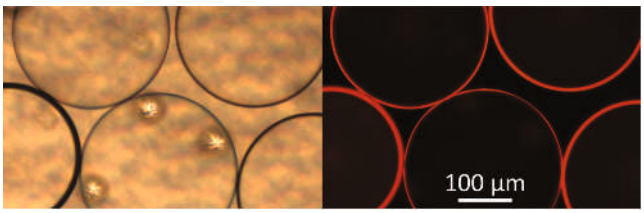

Figure 9. Optical and fluorescence micrographs of various lipid membrane designs formed continuously in the device and collected in one batch. The vesicles were generated by varying the flow rates and geometry as described in Figure 4

batch, thus facilitating the experimental procedure and enhancing reproducibility. Furthermore, since the device is based on commercially available parts with low tolerance, the reproducibility of the device itself is high.

Supporting Information

Electronic Supplementary Material (ESM) with parts for the microfluidic device and additional double emulsion designs is available in the online version at doi: 10.1556/1846.2015.00023.

References

1. Blain, J. C.; Szostak, J. W. *Annu. Rev. Biochem.* **2014**, *83*, 615–640.
2. Zagnoni, M. *Lab Chip* **2012**, *12*, 1026–1039.
3. Matosevic, S. *Bioessays* **2012**, *34*, 992–1001.
4. Karamdad, K.; Law, R. V.; Seddon, J. M.; Brooks, N. J.; Ces, O. *Lab Chip* **2015**.
5. Arriaga, L. R.; Datta, S. S.; Kim, S.-H.; Amstad, E.; Kodger, T. E.; Monroy, F.; Weitz, D. A. *Small* **2014**, *10*, 950–956.
6. Ikonen, E. *Curr. Opin. Cell Biol.* **2001**, *13*, 470–477.
7. Stano, P.; Carrara, P.; Kuruma, Y.; Pereira de Souza, T.; Luisi, P. L. *J. Mater. Chem.* **2011**, *21*, 18887–18902.
8. Allen, T. M.; Cullis, P. R. *Adv. Drug Deliver Rev.* **2013**, *65*, 36–48.
9. Herranz-Blanco, B.; Arriaga, L. R.; Makila, E.; Correia, A.; Shrestha, N.; Mirza, S.; Weitz, D. A.; Salonen, J.; Hirvonen, J.; Santos, H. A. *Lab Chip* **2014**, *14*, 1083–1086.
10. Kong, F.; Zhang, X.; Hai, M. *Langmuir* **2014**, *30*, 3905–3912.
11. Skeie, S. *Int. Dairy J.* **1994**, *4*, 573–595.
12. Rodriguez, N.; Pincet, F.; Cribier, S. *Colloids Surf B.* **2005**, *42*, 125–130.
13. Angelova, M. I.; Dimitrov, D. S. *Faraday Discuss. Chem. Soc.* **1986**, *81*, 303–311.
14. Mathivet, L.; Cribier, S.; Devaux, P. F. *Biophys. J.* **1996**, *70*, 1112–1121.
15. Hope, M. J.; Bally, M. B.; Webb, G.; Cullis, P. R. *Biochim. Biophys. Acta* **1985,** *812*, 55–65.
16. Darszon, A.; Vandenberg, C. A.; Schönfeld, M.; Ellisman, M. H.; Spitzer, N. C.; Montal, M. *Proc. Natl. Acad. Sci.* **1980**, *77*, 239–243.
17. Funakoshi, K.; Suzuki, H.; Takeuchi, S. *J. Am. Chem. Soc.* **2007**, *129*, 12608–12609.
18. Stachowiak, J. C.; Richmond, D. L.; Li, T. H.; Brochard-Wyart, F.; Fletcher, D. A. *Lab Chip* **2009**, *9*, 2003–2009.
19. Xia, Y.; Whitesides, G. M. *Annu. Rev. Mater. Sci.* **1998**, *28*, 153–184.
20. Rossi, F.; Budroni, M. A.; Marchettini, N.; Cutietta, L.; Rustici, M.; Liveri, M. L. T. *Chem. Phys. Lett.* **2009**, *480*, 322–326.
21. Utada, A. S.; Lorenceau, E.; Link, D. R.; Kaplan, P. D.; Stone, H. A.; Weitz, D. A. *Science* **2005**, *308*, 537–541.
22. Shum, H. C.; Lee, D.; Yoon, I.; Kodger, T.; Weitz, D. A. *Langmuir* **2008**, *24*, 7651–7653.
23. Kim, S.-H.; Kim, J. W.; Cho, J.-C.; Weitz, D. A. *Lab Chip* **2011**, *11*, 3162–3166.
24. Foster, T.; Dorfman, K. D.; Ted Davis, H. *J. Colloid Interface Sci.* **2010**, *351*, 140–150.
25. Whitesides, G. M.; Grzybowski, B. *Science* **2002**, *295*, 2418–2421.
26. Nishimura, K.; Suzuki, H.; Toyota, T.; Yomo, T. *J. Colloid Interface Sci.* **2012**, *376*, 119–125.
27. Benson, B. R.; Stone, H. A.; Prud'homme, R. K. *Lab Chip* **2013**, *13*, 4507–4511.
28. Shang, L.; Cheng, Y.; Wang, J.; Ding, H.; Rong, F.; Zhao, Y.; Gu, Z. *Lab Chip* **2014**, *14*, 3489–3493.
29. Duncanson, W. J.; Lin, T.; Abate, A. R.; Seiffert, S.; Shah, R. K.; Weitz, D. A. *Lab Chip* **2012**, *12*, 2135–2145.
30. Tomasi, R.; Noel, J.-M.; Zenati, A.; Ristori, S.; Rossi, F.; Cabuil, V.; Kanoufi, F.; Abou-Hassan, A. *Chem. Sci.* **2014**, *5*, 1854–1859.
31. Walde, P.; Cosentino, K.; Engel, H.; Stano, P. *Chembiochem* **2010**, *11*, 848–865.